

## Modulation Driven Localization of Light in Radially Modulated Optical Lattices

Haitao Wang,<sup>1,2,\*</sup> Wei Jia,<sup>3</sup> Chunhong Qiao,<sup>1</sup> Biyi Wang,<sup>4</sup> and Chengyu Fan<sup>1</sup>

<sup>1</sup> Key Laboratory of Atmospheric Optics, Anhui Institute of Optics and Fine Mechanics, Chinese Academy of Sciences, Hefei Anhui, 230031, China

<sup>2</sup> State Key Laboratory of Pulsed Power Laser Technology, Electronic Engineering Institute, Hefei 230037, China

<sup>3</sup> College of mechanical and electrical engineering, AnHui Jianzhu University, Hefei Anhui, 230031, China

<sup>4</sup> Science and Technology on Electro-optical information Security Control Laboratory, TianJin, 300308, China

\*Corresponding author: [htwang@aiofm.ac.cn](mailto:htwang@aiofm.ac.cn)

---

**Abstract:** We have numerically investigated the periodic optical lattice waveguides driven localization formation of light to tailor the laser filamentary propagating nature. It suggests that the intense nonlinear localization can be observed in the process of lattice tailoring filamentation. We demonstrate that the nonlinear localization is exterior inherit the linear discrete peculiarity, whereas the intrinsic evolution process is responsible for the competition between linear and nonlinear spatiotemporal effects that regulate the spatiotemporal localized nonlinear light bullets propagating configurations. Furthermore, the optimal designed modulation potential drives the transition from stable continuous lattice filament to high-intensity localized propagation mode, which is in favor of extending propagation distance compared with the typical or lattice filament.

**OCIS Codes:** (190.3270) Kerr effect; (260.5950) Self-focusing; (320.2250) Femtosecond Phenomena; (190.7110) Ultrafast nonlinear optics.

---

Date of Submission: 13-09-2017

Date of acceptance: 25-09-2017

---

### I. INTRODUCTION

Femtosecond filamentation has recently received considerable attention in ultra-fast nonlinear optics [1-3]. It has great application value ranging from single-cycle pulse generation to electric discharge triggering and guiding [4], supercontinuum generation, laser-assisted water condensation [5] or aerosol formation [6], remote air lasing [7, 8] and THz radiation [9,10]. Filamentary propagation involves spatial as well as temporal effects. The principle underlying filamentation scenarios is interpreted as dynamic process of a competing pattern resulting both from linear (including diffraction, dispersion) and counter-balance nonlinear optical effects (Kerr self-focusing, plasma defocusing and ionization losses at the laser pulse powers exceeding the critical power of self-focusing). In the linear propagation regime, the beam broadens due to diffraction and dispersion. At high power, the optical Kerr nonlinearity balances the diffraction and a spatial stationary structure is formed. Specifically, spatio-temporal light bullets [11] that can steadily propagate in the anomalous dispersion regime, such as transparent solids, has been obtained [12-14].

However, the propagating patterns of spatial soliton and spatio-temporal light bullets are not steady-state in normal dispersion media (such as in air) [15]. The combined competing actions can lead to a dramatic reshaping of the laser beam itself may either breakup under the effect of the modulational instability or form a filament. To prolong the filament length and to obtain the highly stable filamentation dynamic, a lot of efforts are performed by using of amplitude and phase mask, wave front phase plates, deformable mirrors and lenses [16], or laser pulse temporal reshaping [17]. These widely used technologies mainly depend on changing the parameters of incident laser source. While in most cases, the filamentation processes are associated with strong gradients leading to a non-uniform plasma distribution along the propagating path. Furthermore, the high intensities within the plasma channel make it almost hardly to impose optical impact in order to gain control on filamentation process. Fortunately, a newly method was proposed that filamentation process, by means of photonic lattices [18], which can be formed either transient (like dynamic plasma lattices) or permanently written in the bulk (for instance, in BK7 glass) in the form of an array of waveguides [19, 20], can be well tailored. In contrast to the typical filamentation mechanism, it is found that this filamentation tailoring is not a linear guiding effect but a result of the balance between the nonlinear propagation effects and the linear diffraction induced by the lattice [21].

In this paper, we will further demonstrate that a specific propagation configuration can be formed after

an intense femtosecond laser pulse propagates through the preparative lattice structures. From the spatial and the temporal variations of the propagating pulses, we will show that the lattice waveguides can drive localization formation of light to tailor the filamentation propagating nature. The results shed new light on recent experimental observations, and pave the way for formation of the stabilizing spatio-temporal localization wavepackets, controllable super-continuum generation and pulse reshaping.

## II. NUMERICAL MODEL

The evolution of an electromagnetic field propagation through a dielectric medium is governed by the standard mathematical model — Maxwell's equations, which can be expressed as a set of coupled vector-wave equations containing the electric field  $\mathbf{E}$ , the dielectric displacement field  $\mathbf{D}$  and the current density  $\mathbf{J}$ . For practical scalar version, the Unidirectional Pulse Propagation Equations (UPPE) is an exact system of equations that describes evolution of ultra-short laser pulse along the positive  $z$ -direction for the forward propagating field. In the spectral domain, the canonical modal of the equations can be written as [22]:

$$\frac{\partial \hat{E}}{\partial z} = \left( \frac{i}{2k(\omega)} \nabla_{\perp}^2 + ik(\omega)(1 + \delta n) \right) \hat{E} + \frac{i\omega^2}{2k(\omega)c^2 \epsilon_0} \left( \hat{P}_{NL} + i \frac{\hat{J}}{\omega} \right). \quad (1)$$

In equation (1), the  $\hat{E}$  represents the Fourier presentation of the forward propagation electric field component,  $k(\omega) = n(\omega)\omega/c$  is wave vector and  $n(\omega)$  is the linear refractive index of the material,  $c, \omega$  are light speed and the optical frequency, respectively.  $\hat{P}_{NL}$  is Fourier transform of the nonlinear polarization  $P_{NL}(r, z, t) = 2\epsilon_0 n_0 n_2 I(r, z, t)E(r, z, t)$  in the space-time domain.  $n_0, n_2$  are linear refractive index and nonlinear coefficient at center wavelength  $\lambda_0$  and  $\epsilon_0$  denotes the permittivity of free space, respectively. Take into account the generation of plasma and the photoionization losses, the current density  $J = J_p + J_{pi}$ . In the frequency domain, the free carriers current density by photoionization is treated in terms of Drude model according to the equation:  $\hat{J}_p = c^2 \epsilon_0 \left( \frac{n_0 \sigma(\omega)}{c} + i \frac{\omega_0^2}{c^2 \rho_c \omega (1 + \nu_e^2 / \omega^2)} \right) \times \left( \hat{\rho} \otimes \hat{E} \right)$  and the loss current is  $J_{pi} = \frac{k_0 c^2 \epsilon_0 U_i W(I)}{\omega_0 I} (\rho_0 - \rho) E$ , where  $\nu_e = 1/\tau_c$  and  $\rho_c = \omega_0^2 m_e \epsilon_0 / q_e^2$  is the critical plasma density above which the plasma becomes opaque ( $\rho_c = 1.8 \times 10^{21} \text{ cm}^{-3}$  at  $\lambda_0 = 800 \text{ nm}$ ), here,  $q_e$  and  $m_e$  denote electron charge and mass, respectively,  $\tau_c$  represents the electron collision time. The cross-section for inverse Bremsstrahlung also follows the Drude model and is given by  $\sigma(\omega) = k_0 \omega_0 \tau_c / n_0 \rho_c (1 + \omega_0^2 \tau_c^2)$ .

The evolution of plasma density  $\rho$  is defined in the form:

$$\frac{\partial \rho}{\partial t} = W(I)(\rho_{at} - \rho) + \frac{\sigma(\omega_0)}{U_i} \rho |E|^2 - \alpha \rho^2, \quad (2)$$

where the quantity  $U_i$  and  $\rho_{at}$  denote the molecules ionization potential in air and the neutral gas density, respectively. The multi-photon ionization (MPI) rate obeys the results of Perelomov-Popov-Terent'ev (PPT) ionization model and can be approximately expressed by  $W(|E|^2) \rightarrow W_{MPI} = \sigma_K |E|^{2K}$ ,  $\sigma_K$  denotes the photoionization cross section and  $K = \text{mod}(U_i / \hbar \omega_0 + 1)$  is the minimum number of photons necessary to ionize gas medium and its quantity depends on the gas species.

The input laser pulses are with Gaussian profiles both in the spatial and temporal domain as follows:

$$E(r, t, z=0) = \sqrt{\frac{2P_{in}}{\pi r_0^2}} \times \exp\left\{-\frac{r^2}{r_0^2}\right\} \times \frac{1}{2\pi} \int_{-\infty}^{\infty} d\omega \cdot \exp\left(i \frac{(\omega + \omega_0)r^2}{2cf} + i\omega t\right) \cdot \mathfrak{F}\left[\exp\left(-\frac{t^2}{T_p^2}\right)\right], \quad (3)$$

where  $\mathfrak{F}[E(t)] = \int_{-\infty}^{\infty} dt \cdot \exp\left(-\frac{t^2}{T_p^2}\right) \exp(-i\omega t)$  represents the Fourier transform of the temporal profile of the input pulse. Eq. (3) includes the importance of a frequency dependent lens factor [23] describing the fact that different frequency components of the input pulse have different wavefront curvature and will be diffracted into different cone angles. In the calculation,  $P_{in}, r_0 = 0.5 \text{ mm}, T_p = 35 \text{ fs}$  and  $f$  denote input pulse peak power, beam radius, pulse duration, and effective focal length, respectively.  $k_0 = \omega_0/c = 2\pi n_0/\lambda_0$  and  $\omega_0$  are the wave number and the angular frequency of the carrier wave, respectively. In the simulation, we use the full-width at

half maximum (FWHM)  $t_{FWHM} = \sqrt{2 \ln 2} T_p$  with respect to the intensity and introduce the pulse energy through  $E_{in} = P_{in} T_p \sqrt{\pi/2}$  to characterize the incident pulses.

In equation (1), the important term  $\delta n$  models the contribution of refractive index variation of the nonlinear periodic lattice waveguides, which are full high-dimensional periodic system and can sustain a fertile environment for wave propagation. The focusing or defocusing attribute of two-dimensional periodic lattice structure relies on the sign of nonlinear refractive modulation index. The 3D periodic waveguides from lattice arrays can be an axisymmetrical array structure [18] or a cylindrically symmetrical one [21]. For the latter case,  $\delta n = \Delta n_0 \sum_{m=1}^N F \left[ \sqrt{x^2 + y^2} - \left( m + \frac{1}{2} \right) \Lambda \right]$ , where  $F(r) = \exp\left\{-\left(r/w\right)^{2p}\right\}$  is the function describing the refractive index distribution with a super-Gaussian profile of order  $p = 8$ .  $w = 0.2 r_0 = 100 \mu m$  is the typical width of the distribution.  $\Delta n_0$  and  $\Lambda$  are the modulation depth and period of the lattice, respectively.

### III. DISCUSSIONS

In Fig.1(a), the solid line denotes schematic representation of the relative positions of incident laser beam and cylindrical lattice. The tailoring effects on the propagating beam mainly associates with energy flow manifested by the Poynting vector. In the following discussed cases, the sign of the modulation depth are negative. Lattice waveguide structure Consists of low-index concentric rings. In this architecture type of lattice, light has the tendency to become localized [24, 25], which opens up the opportunity for discrete lattice soliton formation, in the high index areas between the low-index waveguides. It may be understood as the stable mode of the discrete band gap solitons, forming the spatially localized breathers, which propagate along the arrays, when the beam centered between a couple of waveguide arrays. This management configuration leads to the excitation of particular Floquet-Bloch bands [26].

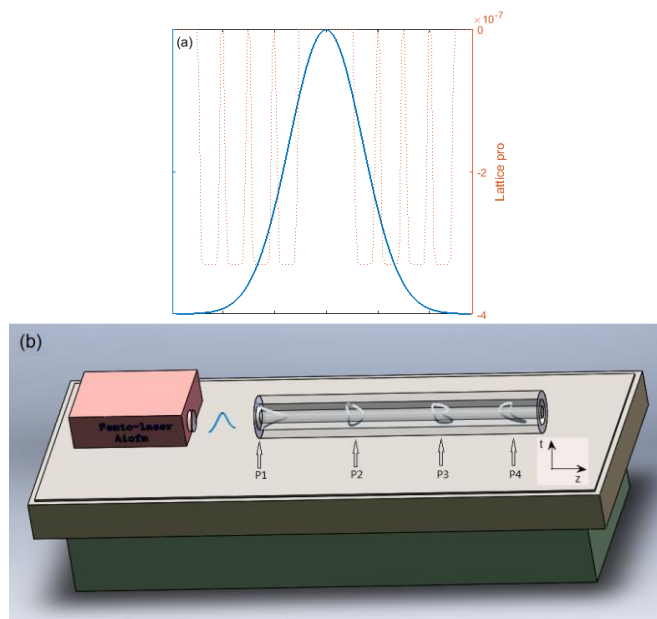


**Fig. 1.** (color online) (a) The relative position of incident laser beam profile in the cylindrical lattice array. (b) Schematic of the 3-dimensional array of diffracting optical lattice-air waveguides, the solid lines denote the temporal profiles of the propagating pulse in the moving coordinate.

To demonstrate a periodic transverse modulation of the refractive index modifies substantially both the linear diffraction and, consequently, strongly affects the nonlinear propagation and localization of light in the form of optical solitons, two propagation regimes, linear and nonlinear, are considered in detail. In the linear propagation regime, the effect of the waveguide structure on pulse propagation mainly limited to diffraction and linear guiding effect. In the nonlinear propagation regime, the ability of the waveguide structure to affect propagation properties of laser pulse is fancily visualized in Fig. 1(b), which presents the envelop shapes of the temporal profiles as a function of the propagation distance. Apparently sensitive to input power, an interplay between periodicity and modulation in lattices provides the possibility for tailoring diffraction and dispersion properties of light as well as controlling nonlinear interactions. Furthermore, the plasma generation, associating with multiphoton absorption (MPA), will be non-negligibly developed and markedly manifest itself by inducing

distortion of the trailing of propagating pulse, due to the local intensity is still above the threshold of ionization. The different physical mechanisms responsible for the dynamic structure formation of intense discrete localization should be further identified.

In order to verify the localization structure is excited in the lattices, we performed numerical simulations to analyze localized formation. At low optical power of  $P_m = 0.07 P_{cr}$ , a focusing nonlinearity can't manifest itself obviously, the beam continues to be decayed by diffraction after a short distance stable propagation in the case of modulation depth  $\Delta n_0 = -3.3 \times 10^{-7}$  and period  $\Lambda = 250 \mu m$  [seen in Fig. 2(a)]. It is clearly shown that the discrete distribution is not formed. However, the propagation configuration is absolutely different from the typical diffraction when a periodic potential is involved along the propagating path, i.e., when the modulation depth is slightly increased up to  $\Delta n_0 = -8 \times 10^{-6}$  while the period of lattice keeps fixed [Fig. 2(b)]. The optical field self-localizes and diffracts discretely, which provides a clear indication of discrete lattice localization formation, in the lattice array. The periodic spatial gap range becomes close between nearest-neighboring discretized optical field, with the increase of the magnitude of the potential depth as high as  $\Delta n_0 = -1.5 \times 10^{-5}$  [Fig. 2(c)], which has a significant effect on the light propagation dynamics in the periodic lattice. It shows that as the refractive index modulation depths of the lattices increase, the light gradually converges in the transverse dimension. The light travels with low diffraction and propagates as unstable multi-point discrete optical solitons, due to the transverse instability of energy fluence, in the periodic lattice waveguide. This is consistent with the prediction of discrete lattice soliton formation [27], when a cylindrical waveguide array is involved along the light propagation path. This also demonstrates that the light can be transversely localized in the linear regime when the modulation depth is high enough.

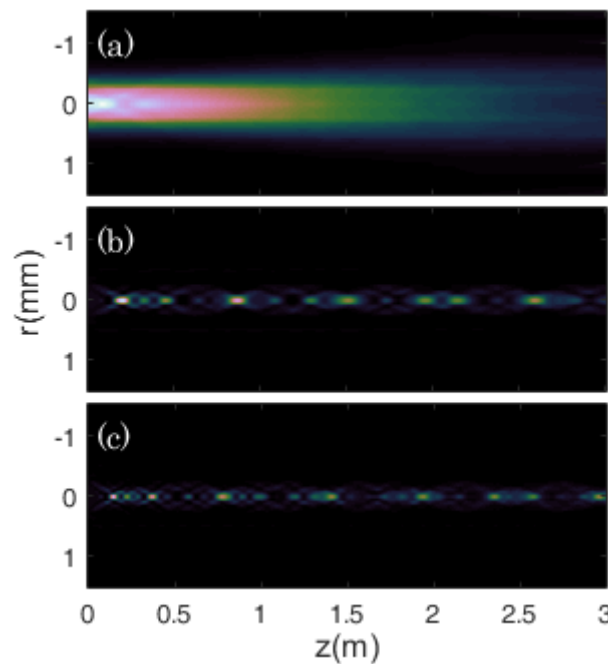


**Fig. 2.** (color online) Transvers profiles of laser beam along the propagating axis for period  $\Lambda = 250 \mu m$  and the modulation depth (a)  $\Delta n_0 = -3.3 \times 10^{-7}$ . (b)  $\Delta n_0 = -8 \times 10^{-6}$ . (c)  $\Delta n_0 = -1.5 \times 10^{-5}$ .

For comparison, discrete diffraction behavior of light in the form of lattice filament case is shown in Fig. 3, when the incident power is high enough into nonlinear propagation regime. For the input power  $P_m = 1.25 P_{cr}$ , modulation period  $\Lambda = 350 \mu m$  and modulation depth  $\Delta n_0 = -3.3 \times 10^{-7}$  [18], a continuous lattice filament [seen in Fig. 3(a)], which the peak intensity drops compared to the typical filamentation dynamics, can be observed. It should be noted that this configuration barely triggers plasma generation with peak intensities less than  $3 \text{ TW/cm}^2$ , as detailed in Fig. 4(a). Interestingly, by slightly increase the optical power to  $P_m = 1.43 P_{cr}$  and other lattice parameters are  $\Lambda = 250 \mu m$  and  $\Delta n_0 = -8 \times 10^{-6}$ , discrete and transversely localized behavior of light [Fig. 3(b)], which is the same image as in the linear regime [Fig. 2(b)], is formed. Furthermore, homogeneous and more intense periodic localization propagation dynamics has been presented in Fig. 3(c), as

the optical power approaches  $3.79 P_{cr}$  and the potential amplitude gets close to  $-1.5 \times 10^{-5}$ . It demonstrates that with the enhancement of the optical power and modulation depth, the beam self-focuses rapidly and the tailoring effect of the interaction of nonlinear self-focusing and diffraction of lattice array makes the spatial localization and the discrete energy distribution become smooth. Practically, most of the energy of the propagating light is still contained in the central high refractive index area. The increasing of the optical power and modulation depth, on the one hand, changes the propagation diagram from linear regime to nonlinear regime. On the other hand, it drives the transition from stable continuous lattice filament to localized propagation mode. With the same power as Fig. 3(c), a classical filamentation pattern computed with a uniform linear refraction index ( $\Delta n_0 = 0$ ) is shown in Fig.3(d). Compared to the original localization pattern of Fig. 3(c), both of them have the same peak intensity level, while the spatial length maintaining clamping intensity [1,2] is very short for the classical filamentation pattern. So the lattice structure is certainly helping to self-guide the pulse and inhibit diffraction there.

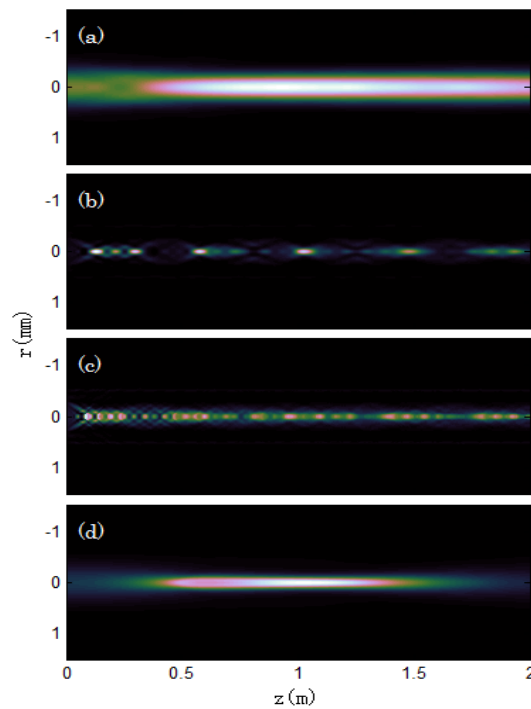


**Fig. 3.** (color online) Transvers profiles of laser beam along the propagating axis for (a)  $P_{in} = 1.25 P_{cr}$ ,  $\Lambda = 350 \mu m$ ,  $\Delta n_0 = -3.3 \times 10^{-7}$ . (b)  $P_{in} = 1.43 P_{cr}$ ,  $\Lambda = 250 \mu m$ ,  $\Delta n_0 = -8 \times 10^{-6}$ . (c)  $P_{in} = 3.79 P_{cr}$ ,  $\Lambda = 250 \mu m$ ,  $\Delta n_0 = -1.5 \times 10^{-5}$ . (d)  $P_{in} = 3.79 P_{cr}$ ,  $\Delta n_0 = 0$ .

It is noted that the increasing of the optical power and modulation depth also results into the increasing of local intensity, which still remains sufficiently high to provide for ionization, corresponding to the generation of plasma associated with MPA. The maximum intensity and electron density can be reached periodically, resulting in relatively flat intensity plateau formation along the propagation axis with gradually increased potential amplitudes, though the profiles are not generally maintained at constant levels [seen in Figs. 4(b) and 4(c)]. After a transient stage of stable light bullets, the beam pattern was observed to relax to a tailored localization with weak energy dissipation along propagation direction. An increasing number of spatial breathe dynamics and temporal pulse-splitting events are obtained for increasing input energies. The crucial effect of MPA and plasma generation suggests that they are responsible for both reducing the intense peak in the central part of the beam and leading to the gradually quasisymmetry splitting event along the propagation axis. This numerically obtained distinctive feature of lattice tailoring filamentation is consistent with what has been proposed in Fig.1(b). The main role of MPA is further confirmed by the fact that red-shifting spectra frequencies were substantially observed after splitting events, whereas plasma defocusing, in combination with self-steepening, would be responsible for the generation of new spectral components on the blue side of the spectrum [28].

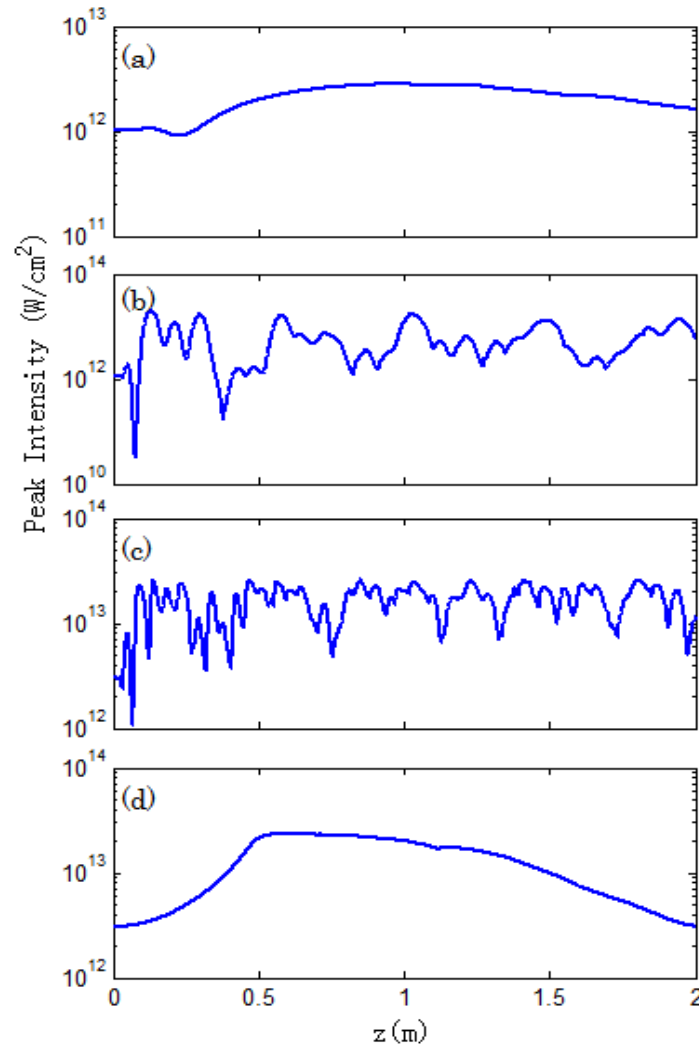


**Fig. 4.** Peak intensities on axis as functions of the propagation distance are plotted with the same parameters as in Figure.3.

#### IV. SUMMARY

We have theoretically and numerically demonstrated intense nonlinear localization of light in the optically-induced photonic lattices where the refractive index is modulated periodically in the transverse direction by properly handle of the optical power and modulation depth. When the incident power is high enough into nonlinear propagation regime, the optical lattice changes the propagation diagram from linear discrete diffraction behavior of light to nonlinear light bullets case. It suggests that the nonlinear localization is exterior inherit the linear discrete peculiarity, whereas the intrinsic evolution process is responsible for the competition between linear and nonlinear spatiotemporal effects that regulate the spatiotemporal localized nonlinear light bullets propagating configurations. Secondly, the modulation drives the transition from stable continuous lattice filament with low peak intensity to high-intensity localized propagation mode. It indicates that the modulation potential is significantly favorable of the formation of spatiotemporal localized nonlinear light bullets, which can propagates rather extended distance compared with the typical or lattice filament, under the conditions of other parameters are the same. This finding will bridges discrete optical propagation with spatiotemporal light bullets formation, especially, in the framework of femtosecond laser filamentation tailoring.

#### ACKNOWLEDGEMENTS.

The project was supported by Open Research Fund of State Key Laboratory of Pulsed Power Laser Technology, Electronic Engineering Institute (Grant Nos: SKL2013KF01 and SKL2015KF03); National Natural Science Foundation of China (Grant No: 61605223) and Dean fund of Hefei Institutes of Physical Science, Chinese Academy of Sciences (Grant No. YZJJ201506).

**REFERENCES**

- [1] A. Couairon and A. Mysyrowicz, “Femtosecond filamentation in transparent media”, *Phys. Rep.* **441**, 47–189, (2007).
- [2] L. Bergé, S. Skupin, R. Nuter, J. Kasparian, J. P. Wolf, “Ultrashort filaments of light in weakly-ionized, optically-transparent media”, *Rep. prog. phys.* **70**, 1633-1713, (2007).
- [3] S. L. Chin, T. J. Wang, C. Marceau, J. Wu, J. S. Liu, O. Kosareva, N. Panov, Y. P. Chen, J. F. Daigle, S. Yuan, A. Azarm, W. W. Liu, T. Seideman, H. P. Zeng, M. Richardson, R. X. Li and Z. Z. Xu, “Advances in Intense Femtosecond Laser Filamentation in Air”, *Laser Physics.* **22**, 1–53, (2012).
- [4] B. Forestier, A. Houard, I. Revel, M. Durand, Y. B. André, B. Prade, A. Jarnac, J. Carbonnel, M. Le Nevé, J. C. de Miscault, B. Esmler, D. Chapuis and A. Mysyrowicz, “Triggering, guiding and deviation of long air spark discharges with femtosecond laser filament”, *AIP ADVANCES.* **2**, 012151, (2012).
- [5] P. Rohwetter, J. Kasparian, K. Stelmaszczyk, et al., “Laser-induced water condensation in air”, *Nature Photonics.* **4**, 451-456, (2010).
- [6] H. Saathoff, S. Henin, K. Stelmaszczyk, M. Petrarca, R. Delagrangé, Z. Q. Hao, J. Lüder, O. Möhler, Y. Petit, P. Rohwetter, M. Schnaiter, J. Kasparian, T. Leisner, J. P. Wolf and L. Wöste, “Laser filament-induced aerosol formation”, *Atmos. Chem. Phys.* **13**, 4593–4604, (2013).
- [7] T-J Wang, J. F. Daigle, J. J. Ju, S. Yuan, R. X. Li, and S. L. Chin, “Forward lasing action at multiple wavelengths seeded by white light from a femtosecond laser filament in air”, *Phys. Rev. A*, **88**(5), 053429, (2013).
- [8] Y. Liu, Y. Brelet, G. Point, A. Houard, and A. Mysyrowicz, “Self-seeded lasing in ionized air pumped by 800nm femtosecond laser pulses”, *Opt. Express* **21**(19), 22791–22798, (2013).
- [9] B. Clough, J. M. Dai and X. C. Zhang, “Laser air photonics: covering the Terahertz gap and beyond”, *Chinese J. Phys.* **52**(1-II), 416-430, (2014).
- [10] V. A. Andreeva, O. G. Kosareva, N. A. Panov, D. E. Shipilo, P. M. Solyankin, M. N. Esaulkov, P. González de Alaiza Martínez, A. P. Shkurinov, V. A. Makarov, L. Bergé, and S. L. Chin, “Ultrabroad Terahertz Spectrum Generation from an Air-Based Filament Plasma”, *Phys. Rev. Lett.* **116**(6), 063902, (2016).
- [11] D. Majus, G. Tamošauskas, I. Gražulevičiūtė, N. Garejev, A. Lotti, A. Couairon, D. Faccio, and A. Dubietis, “Nature of Spatiotemporal Light Bullets in Bulk Kerr Media”, *Phys. Rev. Lett.* **112**(19), 193901, (2014).
- [12] L. Bergé, and S. Skupin, “Self-channeling of ultrashort laser pulses in materials with anomalous dispersion”, *Phys. Rev. E*, **71**(6), 065601, (2005).
- [13] M. Durand, A. Jarnac, A. Houard, Y. Liu, S. Grabielle, N. Forget, A. Durécu, A. Couairon, and A. Mysyrowicz, “Self-guided propagation of ultrashort laser pulses in the anomalous dispersion region of transparent solids: a new regime of filamentation”, *Phys. Rev. Lett.* **110**(11), 115003 (2013).
- [14] S. V. Chekalin, E. O. Smetanina, A. I. Spirkov, V. O. Kompanets, V. P. Kandidov, “Filamentation of a phase-modulated pulse under conditions of normal, anomalous and zero group velocity dispersion”, *Quantum Electronics*, **44** (6), 577 – 584, (2014).
- [15] A. Couairon, “Light bullets from femtosecond filamentation”, *Eur. Phys. J. D* **27**, 159–167 (2003).
- [16] A. A. Ionin, N. G. Iroshnikov, O. G. Kosareva, A. V. Larichev, D. V. Mokrousova, N. A. Panov, L. V. Seleznev, D. V. Sinitsyn and E. S. Sunchugasheva, “Filamentation of femtosecond laser pulses governed by variable wavefront distortions via a deformable mirror”, *J. Opt. Soc. Am. B.* **30**(8), 2257-2262, (2013).
- [17] T. T. Xi, Z. J. Zhao and Z. Q. Hao, “Filamentation of femtosecond laser pulses with spatial chirp in air”, *J. Opt. Soc. Am. B.* **31**(2), 321-324, (2014).
- [18] P. Panagiotopoulos, N. K. Efremidis, D. G. Papazoglou, A. Couairon and S. Tzortzakis, “Tailoring the filamentation of intense femtosecond laser pulses with periodic lattices”, *Phys. Rev. A.* **82**(6), 061803(R), (2010).
- [19] M. Bellec, P. Panagiotopoulos, D. G. Papazoglou, N. K. Efremidis, A. Couairon and S. Tzortzakis, “Observation and Optical Tailoring of Photonic Lattice Filaments”, *Phys. Rev. Lett.* **109**(11), 113905, (2012).
- [20] S. Suntsov, D. Abdollahpour, D. G. Papazoglou, P. Panagiotopoulos, A. Couairon and S. Tzortzakis, “Tailoring femtosecond laser pulse filamentation using plasma photonic lattices”, *Appl. Phys. Lett.* **103** 021106, (2013).
- [21] P. Panagiotopoulos, A. Couairon, N. K. Efremidis, D. G. Papazoglou and S. Tzortzakis, “Intense dynamic bullets in a periodic lattice”, *Opt. Express*, **19**(11), 10057-10062, (2011).
- [22] A. Couairon, E. Brambilla, T. Corti, D. Majus, O. de J. Ramírez-Góngora and M. Kolesik, “Practitioner’s guide to laser pulse propagation models and simulation”, *Eur. Phys. J. Special Topics.* **199**, 5–76, (2011).
- [23] L. Bergé, S. Skupin, and G. Steinmeyer, “Self-recompression of laser filaments exiting a gas cell”, *Phys. Rev. A.* **79**(3), 033838, (2009).
- [24] J. W. Fleischer, M. Segev, N. K. Efremidis and D. N. Christodoulides, “Observation of two-dimensional

- discrete solitons in optically induced nonlinear photonic lattices”, *Nature*. **422**, 147-150, (2003).
- [25] M. Segev, Y. Silberberg and D. N. Christodoulides, “Anderson localization of light”, *Nature Photonics*. **7**, 197-204, (2013).
- [26] Y. L. Qi and G. Q. Zhang, “Linear discrete diffraction and transverse localization of light in two-dimensional backbone lattices”, *Opt. Express* **18**(19), 20170–22798, (2013).
- [27] I. L. Garanovich, S. Longhi, A. A. Sukhorukova, Y. S. Kivshar, “Light propagation and localization in modulated photonic lattices and waveguides”, *Phy. Rep.* **518**, 1–79, (2012).
- [28] H.T. Wang, C.Y. Fan, P. F. Zhang and W. Jia, “Tailoring the plasma channel generated by femtosecond laser pulse”, *J. Opt.* **17**, 025501, (2015).